water

MDPI

Article

CO_2 Degassing in Sicily (Central Mediterranean) as Inferred from Groundwater Composition

Marianna Cangemi [1], Maria Grazia Di Figlia [2], Rocco Favara [2] and Marcello Liotta [2,*]

[1] Dipartimento di Scienze della Terra e del Mare, Università degli Studi di Palermo, via Archirafi 36, 90123 Palermo, Italy; mariannacangemi@gmail.com

[2] Istituto Nazionale di Geofisica e Vulcanologia, Sezione di Palermo, via Ugo La Malfa 153, 90146 Palermo, Italy; difigliam@yahoo.com (M.G.D.F.); rocco.favara@ingv.it (R.F.)

* Correspondence: marcello.liotta@ingv.it; Tel.: +39-091-6908403

Received: 26 May 2020; Accepted: 5 July 2020; Published: 10 July 2020

Abstract: The circulation of groundwater is influenced by several factors, including permeability changes due to the dynamics of the stress field acting along tectonic discontinuities. Open faults can act as preferential pathways for the escape of crustal and subcrustal gases, such as CO_2, towards the surface, allowing their chemical interaction with meteoric fluids. Here, we present the first map of dissolved CO_2 partial pressure in the groundwater of Sicily, Italy. Based on the chemical analysis of 557 samples of groundwater, which were collected in wells and springs, we calculated the related CO_2 partial pressure (PCO_2) using PHREEQC software. The spatial distribution of the calculated PCO_2 values highlights a general homogeneity at the regional scale, interrupted by positive anomalies linked to the main seismogenic or volcanic areas. Faults work as preferential escape pathways for deep CO_2. The subsequent CO_2–water–rock interaction determines the chemical composition of circulating water. As a consequence, groundwater composition can be successfully used to identify anomalous degassing areas.

Keywords: Sicily; groundwater; PCO_2

1. Introduction

The chemical composition of groundwater is the result of a series of complex interaction processes occurring between natural waters, rocks, and gases, being strictly influenced by the atmosphere and biosphere. A huge number of different geochemical reactions occur in geological systems, rationalized by a finite array of reactions able to describe the sequences of states of aqueous solution composition, speciation, and mineral paragenesis over time [1]. Previous studies addressed the modeling of reactions governing silica phases and aqueous solutions [2–6], or carbonate aquifer systems, focusing on the interactions between minerals and aqueous species, their effects on water composition, and residence times [7–9].

Sicily is characterized by the presence of sedimentary, metamorphic, and volcanic rocks, mainly composed of carbonates, silicates, and alkali sulfate evaporites. Primary minerals are dissolved and/or altered during the chemical interaction with groundwater and dissolved gases.

Several processes contribute to CO_2 dissolution in groundwater. It can be generated from biodegradation of organic matter in the soil. Otherwise, metamorphic zones can release abundant CO_2 produced by high-temperature metamorphism of carbonates to groundwater [10]. Furthermore, CO_2 is the major gas species, after water vapor, released by volcano-magmatic processes, because it is the first gas to be exsolved from a magmatic melt due to its low solubility [11].

Carbon dioxide travels from the depths to the surface following discontinuities, generally constituted of deep faults, interacting with shallow aquifers [12]. Consequently, dissolved CO_2 is a valuable geochemical indicator of volcanic and seismic processes (e.g., [13–19]).

In central Italy, Chiodini et al. [20] showed that the influx of deep CO_2 into the overlying groundwater yields a widespread PCO_2 anomaly in the aquifer. Furthermore, De Paola et al. [21] suggest that coseismic decarbonation can produce detectable PCO_2 anomalies in shallow groundwater.

These kinds of processes can be usefully investigated in Sicily, as it is characterized by seismically active areas, such as in eastern Sicily, which has intense strong crustal degassing (mofette and mud volcanoes) as well as deep input of CO_2 by mantle degassing [22], volcanic degassing (eastern Sicily with Mount Etna and the Hyblean Plateau), or metamorphic decarbonation in the Peloritani mountain range [23]. Several hydrothermal systems have been recognized in Sicily, located in the northeast (Alì, Acireale, Castroreale) as well as in the western sector of the island (Termini Imerese, Trabia, Cefalà Diana, Chiusa Sclafani, S.G. Gemini) [24,25]. Significant CO_2 degassing also occurs in the main Sicilian carbonate aquifers, such those of the Iblei (southeast), Madonie (northwest), Sicani (central-west), and Palermo–Trapani (northwest) mounts [10,24–27].

The aim of this work was to depict a regional framework of the CO_2 content of groundwater. We used chemical data from the "Piano di Tutela delle Acque" (Water Protection Plan) of the Sicilian Regional Government (INGV, 2005), inferring PCO_2 from pH and alkalinity, assuming equilibrium between carbonate species. Particular attention was paid to the possible relationship between anomalous CO_2 content and the tectonic and volcano–tectonic structures intercepting these aquifers.

2. Geological Background

Sicily, located along the main Eurasia–Nubia convergent plate boundary [28–30], represents a segment linking the African Maghrebides with the Southern Apennines across the Calabrian accretionary wedge. Three main elements mark both the collisional complex of Sicily and its offshore continuation: (i) the Hyblean Foreland outcropping in southeastern Sicily; (ii) the Caltanissetta Basin, a dynamic foredeep basin of Late Miocene to Quaternary age; and (iii) a complex chain, thrust towards the east and southeast, consisting of the Calabrian Arc and the Maghrebian thrust belt ([31] and references therein). The Hyblean Foreland, submerged by the Pelagian Sea and the adjacent Ionian Sea, represents a remnant of a Late-Jurassic–Early-Cretaceous passive continental margin. The Caltanissetta Basin, located along the northern side of the foreland, is presently buried by the frontal sector of the chain formed of an E and SE vergent fold and thrust belt, outcropping on land and submerged in the adjacent seas. It is made of a "European" element (Peloritani Units), a "Tethyan" element (Sicilide Units), and an African element (Maghrebian Sicilian Units) [32–36]. The different elements evolved in a tectonic framework characterized by two main compressional phases [33,37]: (i) the first one occurred during the Middle–Late Miocene, which caused the overthrusting of the deep-water carbonate above the not-already-deformed carbonate platform substrate; (ii) the latter is of Pliocene to Lower Pleistocene age, during which the carbonate platform units were deformed throughout deep-seated structures, reimbricating the previously emplaced deep-water carbonates. Simultaneously, thrust, backthrust, and lateral displacements [38], together with clockwise paleomagnetically detected nappe rotations (Late-Miocene–Middle-Pleistocene) created a wedge top basin filled with syntectonic deposits [34,37,39]. Details about lithostratigraphy can be found in Basilone [40].

Volcanism has occurred since the Late Triassic times in western Sicily ([41] and references therein) and in the Iblean area [42,43]. Etna is a prominent recent example of active basaltic volcanism in Sicily ([44] and references therein).

Major earthquakes presently occur in eastern Sicily ([30] and references therein), along the NNW-trending offshore fault system located between Siracusa and Catania, parallel to the Malta Escarpment and to the transtensional fault zone separating Sicily from the Ionian abyssal plain [45,46]. Another zone of medium- to high-magnitude earthquakes is along the E-W trending compressive belt in the southern Tyrrhenian Sea ([47] and references therein). Moreover, contractional to transpressional

mechanisms have been recorded in southwestern Sicily [48]. Finally, in the northeastern Sicily belt (Madonie–Peloritani) and beneath the Caltanissetta Basin, extensional to transtensional mechanisms have been recorded.

3. Materials and Methods

Data used in this work refer to physicochemical parameters and concentrations of dissolved ions taken from different literature sources, namely, the "Piano Tutela Acque Regione Siciliana" ([10,49,50], integrated with previously unreleased data for western Sicily (courtesy of Paolo Madonia, INGV, Sezione di Palermo)), for a total of 618 groundwater samples.

Gaseous CO_2 dissolution in water occurs due to the following reaction:

$$CO_{2(gas)} + H_2O \leftrightarrow CO_{2(aq)} + H_2O. \quad (1)$$

Since the equilibrium of this reaction is shifted towards the left side and $CO_{2(gas)}$ can be expressed as PCO_2, its constant can be written as

$$K_H = \frac{PCO_2}{CO_{2(aq)}}. \quad (2)$$

$CO_{2(aq)}$ reacts with water (hydration), forming H_2CO_3 following the reaction

$$CO_{2(aq)} + H_2O \leftrightarrow H_2CO_{3(aq)}. \quad (3)$$

We can define H_2CO_3* as the sum of dissolved $CO_{2(aq)}$ and H_2CO_3 [51], and since H_2CO_3 is only 0.16% of $CO_{2(aq)}$ and the reaction rates are so fast with respect to the average residence times of groundwater, we can neglect H_2CO_3 and write the following expression:

$$CO_{2(aq)} = {H_2CO_3}^*. \quad (4)$$

Following Equation (4), the protolysis of carbonic acid can be expressed as

$${H_2CO_3}^* \leftrightarrow H^+ + {HCO_3}^-, \quad (5)$$

the equilibrium of which constant is given by

$$K^* = \frac{\left[H^+\right][{HCO_3}^-]}{{H_2CO_3}^*}. \quad (6)$$

Combining Expressions (2) and (6), we have

$$PCO_2 = \frac{\left[H^+\right][{HCO_3}^-]K_H}{K^*}. \quad (7)$$

Referring to (7), the logarithmic expressions is as follows:

$$Log[PCO_2] = Log\left[H^+\right] + Log[{HCO_3}^-] + Log[K_H] - Log[K^*] \quad (8)$$

$$-Log[PCO_2] = pH - Log[{HCO_3}^-] - Log[K_H] + Log[K^*]. \quad (9)$$

Hence, it is possible to calculate the partial pressure of CO_2 starting from pH and alkalinity using the constants K_H and K_1 once the temperature is known.

Based on the above-described approach, we calculated the partial pressure of CO_2. We processed our data using PHREEQC software [52].

The PCO_2 contour map was realized using Golden Software Surfer (release 13), with the kriging interpolation algorithm. In order to avoid pseudofeatures due to missing data, we separated the sampling points into 4 groups (Western Sicily, Madonie Mountains, Piazza Armerina area, and Eastern Sicily), computing the contouring separately for each area and plotting the results on the same base map; points were separated using the spatial queries options implemented in Qgis software (release 2.18). In order to investigate the potential relationship between the spatial pattern of dissolved CO_2 anomalies and tectonics, we used data from the "Catalogo Parametrico dei Terremoti Italiani" (CPTI15; [53]) reporting locations of high-magnitude historical earthquakes (1000-2014 A.D.) (see cited reference for details). Moreover, we used the most advanced seismogenic source model, namely, the "Database of Individual Seismogenic Sources" (DISS Working Group, 2018), which lists active faults that can generate Mw 5.5 and larger earthquakes, classified as Individual (ISS) or Composite (CSS) Seismogenic Sources. In particular, we looked for the potential role of active faults in releasing CO_2 to aquifers by analyzing Locations of historical earthquakes and seismogenic sources.

4. Results and Discussion

4.1. Physicochemical Composition of Groundwater

Due to the huge amount of data, the main statistical parameters for pH, total alkalinity, PCO_2, major dissolved ions, and SI calcite were computed for all samples and are reported in Table 1 (the full datasets are available in [49]).

A normal probability plot (PP) was used to identify populations of data. This type of plot expresses the probabilities of cumulative frequencies of the measured major elements dissolved in the groundwater. Data that are normally distributed plot along a straight line. Therefore, the presence of multiple straight lines with different slopes indicates the presence of various populations of normally distributed data with diverse origins of the element considered [18]. They show up as extreme points at either end of a probability plot. Figure 1 shows PPs for all major elements, while Table 2 summarizes all identified populations for every major element with the respective threshold values and the percentage of populations recognized. The graphs also indicate the threshold values deduced from the inflection points.

Each element shows a polymodal distribution (Figure 1). Four populations are recognized for the main ions, except for sodium with five populations, and magnesium with three. Generally, the anomalous populations (population IV) concern about 1% of the data; only sodium shows two anomalous populations (IV and V). Population I, defined by lowest concentrations, represents less than 20% of the samples. For magnesium and chlorine, population I is characterized by 96% and 50%, respectively. Population II (intermediate groups) represents more than 40% of the complete dataset.

Table 1. Main statistical parameters of CO_2 partial pressure (PCO_2), pH, saturation index, and major element concentrations.

	pH	**Alk**	**Na**	**K**	**Ca**	**Mg**	**Cl**	**NO_3**	**SO_4^-**	***P*CO_2**	**SI**
		meq·L^{-1}	**mmol·L^{-1}**	**mmol·L^{-1}**	**mmol·L^{-1}**	**mmol·L^{-1}**	**mmol·L^{-1}**	**mmol·L^{-1}**	**mmol·L^{-1}**	**Atm**	**Calcite**
Number of values	618	618	618	618	618	618	618	618	618	618	618
Minimum	5.68	1.20×10^{-1}	1.80×10^{-1}	0.00	5.85×10^{-2}	1.70×10^{-2}	3.01×10^{-2}	0.00	2.00×10^{-2}	2.50×10^{-4}	−4.47
Maximum	8.92	6.68×10	3.06×10^{2}	8.62	3.12×10	2.79×10	3.60×10^{2}	2.05	3.71×10	3.37	1.47
Mean	7.34	5.38	6.54	2.50×10^{-1}	2.95	1.60	6.77	1.29×10^{-1}	1.56	3.21×10^{-2}	0.11
Median	7.34	4.85	1.51	1.00×10^{-1}	2.18	9.34×10^{-1}	1.21	3.57×10^{-2}	5.60×10^{-1}	1.17×10^{-2}	0.16
Average deviation	0.28	1.80	8.08	2.57×10^{-1}	1.66	1.28	8.84	1.45×10^{-1}	1.60	3.60×10^{-2}	0.27
Standard deviation	0.39	3.65	2.38×10	6.30×10^{-1}	2.85	2.45	2.75×10	2.39×10^{-1}	3.39	1.66×10^{-1}	0.51

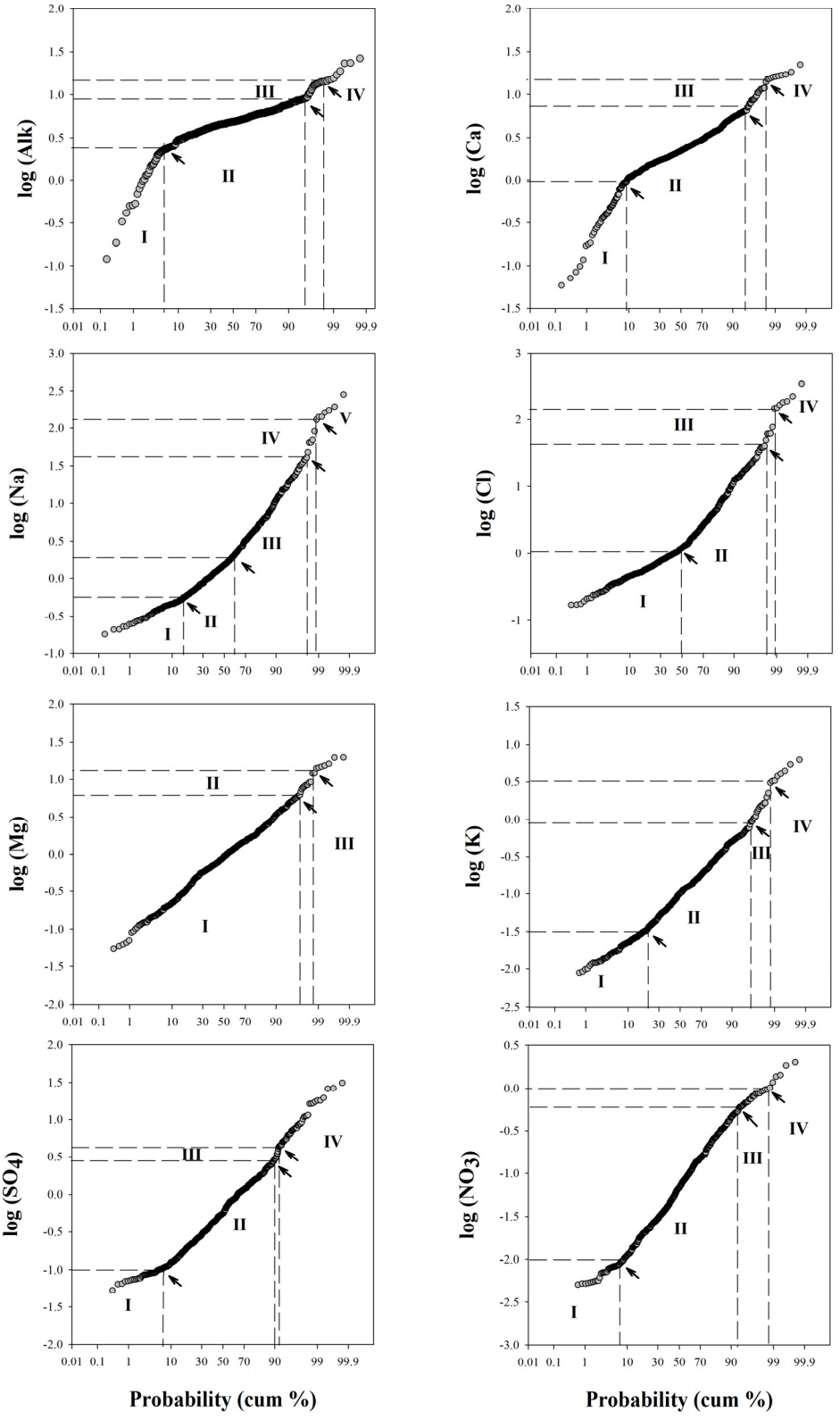

Figure 1. Normal probability plots (PPs) for every major element.

Table 2. Main identified populations and relative percentage and threshold value for all major elements.

	I %	Threshold Value	II %	Threshold Value	III %	Threshold Value	IV %	Threshold Value	V %
Alk meq·L^{-1}	5.5	2.69	89.5	8.9	2	14.8	3		
Na mmol·L^{-1}	16	0.56	43	2	39	40	0.8	126	1.2
K mmol·L^{-1}	21	0.03	75	0.83	2.8	3.24	1.2		
Ca mmol·L^{-1}	9	0.85	85	7.1	4	14.8	2		
Mg mmol·L^{-1}	96.8	6.02	2	13.1	1.2				
Cl mmol·L^{-1}	50	1.12	47	39.8	1.8	147.9	1.2		
NO_3 mmol·L^{-1}	7.4	0.01	85.6	0.61	5.6	1.02	1.4		
SO_4 mmol·L^{-1}	7.1	0.1	82.9	2.8	1.7	4.2	8.3		

The PP for total alkalinity shows three inflection points, reflecting four populations of data with normal distribution: a low concentration group (population I), an intermediate group (population II), and two groups with high concentration values (populations III and IV). Most of the samples belong to population II, which represents 89.5% of the samples, while the highest concentration groups represent only 5%. Most of the waters falling in population IV also show the highest levels of PCO_2. They are located in the volcanic area of Mount Etna, around the volcanic edifice or in the Catania Plain (Naftia, Acqua Grassa, Acque Difesa). Other points fall in areas where hydrothermal activity is recognized, such as the Peloritani mountain range (Ali Terme, Terme Vigliatore). These considerations suggest a link between the total alkalinity of groundwater and the input of deep inorganic CO_2, as also proposed by Grassa et al. [10]. Calcium (Ca) and total alkalinity (Alk) show a similar distribution of various populations of data. As shown in Figure 2, there is a direct relationship between Ca^{2+} + Mg^{2+} and the total alkalinity. High Ca^{2+} and Mg^{2+} levels in groundwater are mainly present where carbonatic aquifers occur, pointing to the water–rock interaction as the source of these dissolved ions. Most of the samples fall around the line 1:1, indicating that CO_2 plays a main role in determining the amount of dissolved ions. Some samples from hydrothermal areas (Termini Imerese, Terme Selinuntine) fall with a cation excess far from the calcite–water equilibrium line, indicating other source processes responsible for the dissolved ions. Accordingly, for these samples, a clear seawater (SW) contribution has been recognized [10,25].

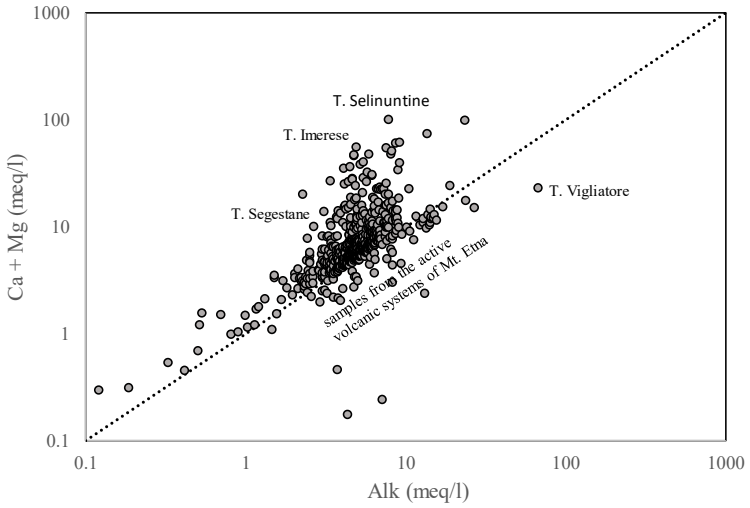

Figure 2. (Ca + Mg) vs. total alkalinity (Alk) concentration expressed as meq·L^{-1} in log scale.

PPs for sodium (Na) and chlorine (Cl) show a similar distribution for low concentrations with three inflection points, reflecting four populations of data: about 47% of samples show an intermediate concentration group (population II), and a reduced group (about 1%) shows higher concentrations (population IV). Only sodium shows an additional population with strongly anomalous values (population V), the sampling points of which (Naftia, Terme Selinuntine, Terme Vigliatore, T. Imerese,

Sclafani Bagni, G. Cassibile) are in some cases located where volcanic or hydrothermal activity has been identified [10,24,25]. In the diagram of Na-Cl (Figure 3), samples containing seawater contributions can be clearly identified. Moreover, according to Grassa [10], the water–silicate minerals interaction coupled with an inflow of CO_2-rich gas to groundwater is responsible for the removal of alkaline earth elements due to the formation of carbonate or silicate alteration minerals in Naftia and Terme Vigliatore. This was also evident in most of the waters located in the active volcanic systems of Mount Etna. However, the Na/Cl molar ratio for most of the samples falls along the typical seawater molar ratio line, with contributions from both maritime aerosols and direct seawater, particularly in sampling points close to the coast (Figure 3). Data of rainwater used in Figure 3 are from [54], in particular, the OVS sample from Mount Vesuvius, representative of rainwater not influenced by volcanic activity and with a low contribution of anthropogenic sources.

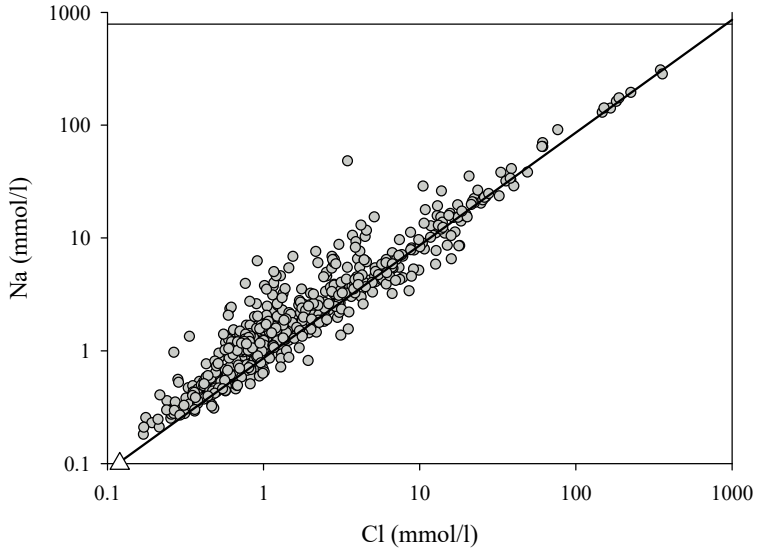

Figure 3. Na vs. Cl ratio as mmol·L^{-1} in log scale. Solid line is Na/Cl ratio for seawater. White triangle is Na/Cl ratio in meteoric water (data from [54]).

Figure 4 shows the total alkalinity plotted against the sum of the cation equivalents (ΣCat). Since CO_2-driven weathering should give a direct positive correlation between the two parameters (e.g., [55]), the graph allows one to recognize the role of the weathering process as a source of metals dissolved in groundwater. However, all of the samples deviate from the 1:1 line, exhibiting an excess of cations and suggesting the influence of other processes determining the chemical composition of groundwater. This is particularly evident in the waters from hydrothermal and volcanic areas.

Saturation indexes of calcite (Figure 5) for these waters indicate that most of the samples are close to the equilibrium saturation or oversaturated with respect to calcite, while the remaining waters are undersaturated to strongly undersaturated ($-4.47 < SI < -1.2$), such as in some of the springs located in the Peloritani area. Dongarrà et al. [56] also found low saturation indexes of calcite up to −3.3 in some waters of the southeastern sector of the Peloritani area, associated with a low degree of mineralization of these waters, suggested by the authors as the result of short contact time with soil and host rocks. Water samples from the volcanic area of Mount Etna (around the volcanic edifice or in the Catania Plain) with highest computed dissolved PCO_2 are characterized by a volcanogenic CO_2-anomalous degassing area [18] and show slight undersaturation in view of calcite. For two samples belonging to the Etnean aquifer, Grassa et al. [10] also suggested a weak water–rock interaction due to short residence time.

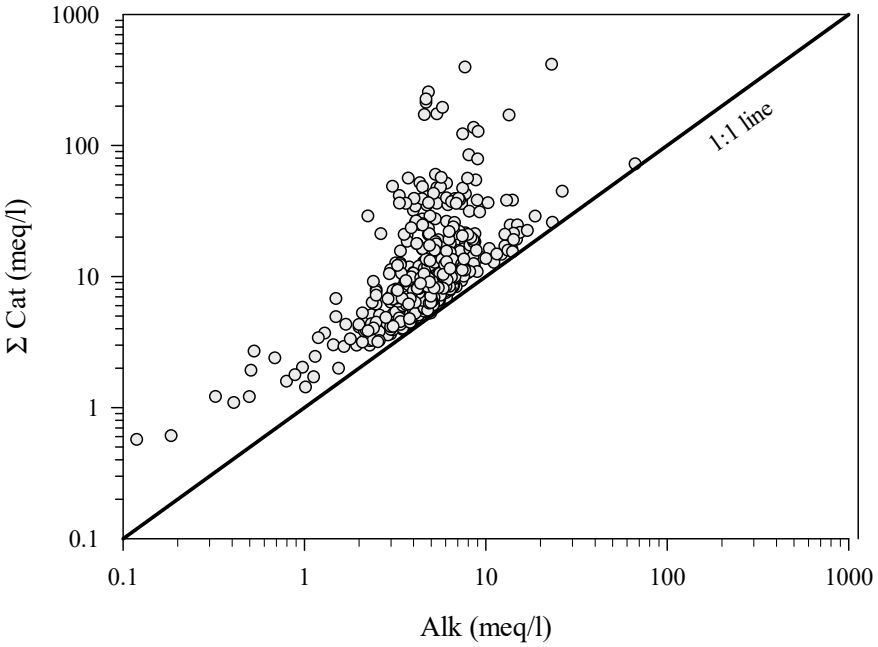

Figure 4. Sum of the cation equivalent versus total alkalinity (Alk). Data as meq/l in log scale.

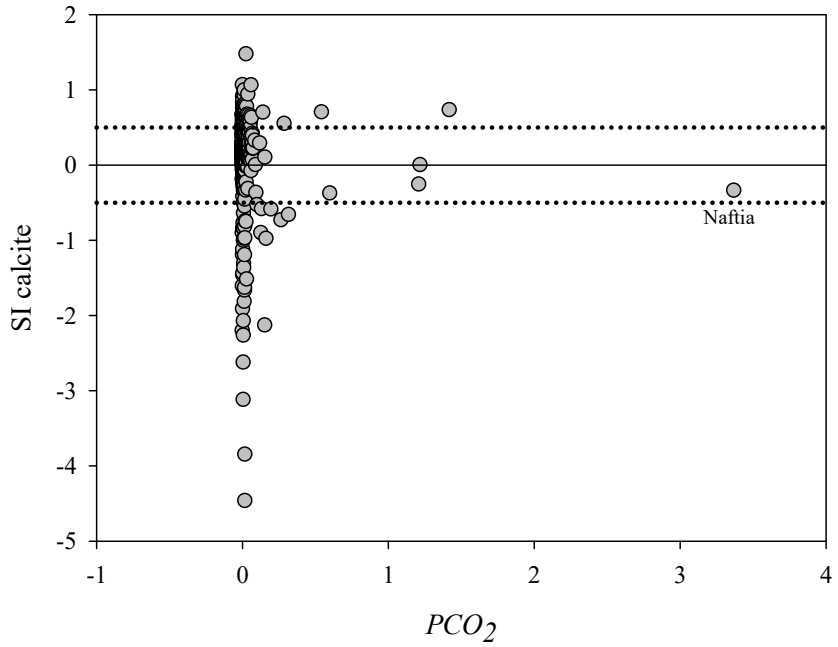

Figure 5. Saturation indexes (SIs) for calcite versus PCO_2.

In spite of the wide variability of the chemical composition of the groundwater, the CO_2 partial pressure solely depends on gaseous CO_2 interacting with groundwater, and its spatial distribution can provide useful information to identify anomalous degassing areas.

4.2. Distribution of Dissolved CO_2 Partial Pressure

Apart from minor anomalies related to a limited number of measures deprived of adequate statistical reliability, it is possible to distinguish different areas (Figure 6) where dissolved CO_2 partial pressure shows levels above the regional background. These are (i) an area aligned N-S between the Castellammare Gulf, in the north, and Sciacca, in the south; (ii) two areas, one on the Tyrrhenian and the other on the Ionian sides of the Peloritani mountains; (iii) the Etna area and Catania Plain that,

albeit with a certain articulation, extends to the northern extremity of the Hyblean Plateau; (iv) the area located close to the Augusta harbor; and (v), finally, an area with two anomalies in the southern side of the Hyblean Plateau.

In terms of amplitude, the strongest anomalies are observed in eastern Sicily and, in particular, along the Ionian side of the Peloritani mountains, in an area of the Catania Plain and in the northern portion of the Hyblean Plateau.

Regarding Figure 6, good agreement is observed between the spatial distribution of seismogenic structures and main dissolved CO_2 partial pressure anomalies.

Moving from west to east, the area hit by the 1968 Belice earthquake (and related seismogenic structures) falls in the middle of the main dissolved CO_2 anomaly of western Sicily. Here, Caracausi et al. [22] recognized three main thermal systems by using $^3He/^4He$ ratios and heat flux data: Alcamo, Sciacca, and Montevago. These are linked to tectonic discontinuities—cutting the continental crust into a regime of differential shortening, oblique thrusting, and clockwise rotations [57]—which convey mantle volatiles to the surface.

The second area is composed of two coupled anomalies lying along the Tyrrhenian and Ionian sides of the Peloritani mountains, respectively. The northern anomaly is delimited northwards by the offshore segment of the Aeolian–Tindari–Letojanni Fault System (ATLFS, [58]). The southern anomaly is delimited southwards by the onshore segment of the ATLFS and eastwards by the seismogenic structure responsible for the 1908 Stretto di Messina earthquake.

The area surrounding Mount Etna shows a wide CO_2 anomaly, which extends southwards reaching the SSW-NNE tectonic structure coinciding with the front of the Sicilian chain–foredeep system. A secondary anomaly is found at the intersection between this front and a N-S active tectonic lineament (Scicli Line, [59] and references therein); this anomaly corresponds to an area interpreted by some authors [60,61] as a southward extension of the wide degassing system of Mount Etna. The high dissolved CO_2 partial pressures recorded here, following this interpretation, are related to volatiles carried by the magmatic gas phase continuously dissolving into shallow aquifers.

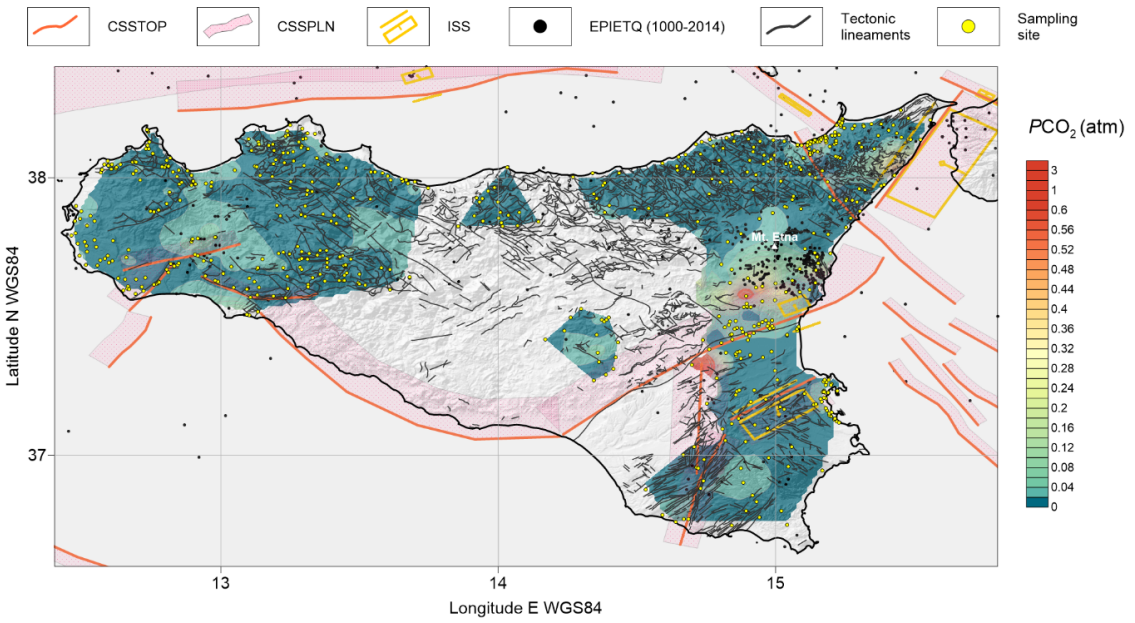

Figure 6. Combination of CO_2 dissolved partial pressure distribution, historical earthquakes (grey circles, EPIETQ) taken from the "Catalogo Parametrico dei Terremoti Italiani, versione CPTI15 [53], top traces of composite seismogenic sources (CSSTOP), dipping plane of composite seismogenic sources (CSSPLN), individual seismogenic sources (ISS) taken from the Database of Individual Seismogenic Sources (DISS, Version 3.2.1, [62]), and tectonic lineaments (from [63]).

Moving eastward, we found another anomaly at the NE border of the 1693 Val di Noto earthquake seismogenic source, located in the immediate hinterland of the Augusta Gulf, close to the onshore prolongation of the Hyblean–Malta escarpment. A final anomalous, hourglass-shaped area is found in the south of the Hyblean Foreland around another tectonic structure connecting the Val di Noto seismogenic source with the N-S lineament previously described (Scicli Line, [59]). Grassa [10] found concentrations and isotope ratios of helium dissolved in groundwater from these areas compatible with a mixing between crustal and MORB fluids, which he indicated to be the result of the uprising of deep fluids along local active tectonic structures.

5. Conclusions

CO_2 emissions are usually determined through the direct measurement of gaseous CO_2 fluxes at the soil–atmosphere interface. However, due to its high solubility in water [64], CO_2 easily dissolves in water and favors water–rock interactions. Consequently, deep CO_2 inputs can be recognized in groundwater composition.

Starting from the chemical composition of groundwater, we calculated the related PCO_2, extending our analysis to all the sectors of Sicily where sampling points were available (557 samples collected from both wells and springs). We presented our results as a matched map of PCO_2 contour lines, locations of historical earthquakes, tectonic lineaments, and seismogenic sources.

The spatial relationship between these elements highlighted anomalous PCO_2 areas, emerging from the regional background, linked to the main seismogenic or volcanic structures. This indicates that the observed anomalies can be ascribed to deep CO_2 degassing sustained by magmatic and hydrothermal activities.

These anomalous areas are: (i) an area aligned N-S between the Castellammare Gulf, in the north, and Sciacca, in the south; (ii) two areas, one on the Tyrrhenian and the other on the Ionian sides of the Peloritani mountains; (iii) the Etna area and Catania Plain extending to the northern extremity of the Hyblean Plateau; (iv) the area located close to the Augusta harbor; and (v) the southern side of the Hyblean Plateau.

In seismogenic areas, groundwater circulation can be affected by permeability variations driven by the dynamics of the stress field. Open faults work as preferential escape pathways for deep CO_2, fostering its chemical interaction with shallower meteoric waters and generating the observed anomalies.

Our results point out that the sampling and chemical analysis of groundwater and subsequent data processing is an efficient and fast method to detect anomalous degassing areas and their relationship with tectonics.

This also implies that the long-term monitoring of groundwater composition could provide some useful information on CO_2 emission variations over time. However, since the groundwater composition also depends on other exogenous processes (e.g., rainfall amount, seawater intrusion, volcanic activity, etc.), data from long-term monitoring programs have to be carefully evaluated in order to avoid overinterpretation of the data.

A step forward after the identification of anomalous CO_2 degassing areas is a deep geochemical investigation based on the chemical and isotope composition of dissolved gases, which would allow for better constraining of the CO_2 source. Furthermore, strontium isotope investigations can provide useful scientific evidence to evaluate the origin of deep brines (e.g., [65]).

Here, we highlight that the proposed approach does not require time-consuming activity in the field and can be carried out with the most common analytical instruments used to determine the chemical composition of groundwater.

Finally, we believe that such an approach can provide a useful tool not only for the scientific community but also for government decision makers. Indeed, the understanding of the geological processes occurring around us represents a good opportunity to make responsible decisions. We suggest that similar geochemical explorations should be extended to the entire national territory.

Author Contributions: The following statements should be used "Conceptualization, M.L.; methodology, M.C. and M.G.D.F.; software, M.C. and M.G.D.F.; validation, M.C., M.G.D.F., and M.L.; data curation, M.C. and M.G.D.F.; writing—original draft preparation, M.C., M.G.D.F., M.L., and R.F.; writing—review and editing, M.C., M.G.D.F., and M.L.; project administration, R.F.; funding acquisition, R.F. All authors have read and agreed to the published version of the manuscript.

Funding: This research was funded by Regione Siciliana, Commissario Delegato per l'Emergenza Bonifiche e la Tutela delle Acque in Sicilia.

Acknowledgments: Thanks are due to the working group of INGV, Sezione di Palermo for sampling and analyses of groundwater.

Conflicts of Interest: The authors declare no conflict of interest. The funders had no role in the design of the study; in the collection, analyses, or interpretation of data; in the writing of the manuscript; or in the decision to publish the results.

References

1. Helgeson, H.C. Evaluation of irreversible reactions in geochemical processes involving minerals and aqueous solutions—I. Thermodynamic relations. *Geochim. Cosmochim. Acta* **1968**, *32*, 853–877. [CrossRef]
2. Marini, L.; Ottonello, G.; Canepa, M.; Cipolli, F. Water-rock interaction in the Bisagno valley (Genoa, Italy): Application of an inverse approach to model spring water chemistry. *Geochim. et Cosmochim. Acta* **2000**, *64*, 2617–2635. [CrossRef]
3. Marini, L.; Canepa, M.; Cipolli, F.; Ottonello, G.; Zuccolini, M. Use of stream sediment chemistry to predict trace element chemistry of groundwater. A case study from the Bisagno valley (Genoa, Italy). *J. Hydrol.* **2001**, *241*, 194–220. [CrossRef]
4. Aiuppa, A.; Federico, C.; Allard, P.; Gurrieri, S.; Valenza, M. Trace metal modeling of groundwater–gas–rock interactions in a volcanic aquifer: Mount Vesuvius, Southern Italy. *Chem. Geol.* **2005**, *216*, 289–311. [CrossRef]
5. Marini, L. Geological sequestration of carbon dioxide—Thermodynamics, kinetics, and reaction path modeling. *Develop. Geochem.* **2005**, *11*, 453.
6. Federico, C.; Pizzino, L.; Cinti, D.; De Gregorio, S.; Favara, R.; Galli, G.; Giudice, G.; Gurrieri, S.; Quattrocchi, F.; Voltattorni, N. Inverse and forward modelling of groundwater circulation in a seismically active area (Monferrato, Piedmont, NW Italy): Insights into stress-induced variations in water chemistry. *Chem. Geol.* **2008**, *248*, 14–39. [CrossRef]
7. Capaccioni, B.; Didero, M.; Paletta, C.; Salvadori, P. Hydrogeochemistry of groundwaters from carbonate formations with basal gypsiferous layers: An example from the Mt Catria Mt Nerone ridge (Northern Appennnines, Italy). *J. Hydrol.* **2011**, *253*, 14–26. [CrossRef]
8. Morgantini, N.; Frondini, F.; Cardellini, C. Natural trace elements baselines and dissolved loads in groundwater from carbonate aquifers of central Italy. *Phys. Chem. Earth, Parts A/B/C* **2009**, *34*, 520–529. [CrossRef]
9. Frondini, F. Geochemistry of regional aquifer systems hosted by carbonate-evaporite formations in Umbria and southern Tuscany (central Italy). *Appl. Geochem.* **2008**, *23*, 2091–2104. [CrossRef]
10. Grassa, F.; Capasso, G.; Favara, R.; Inguaggiato, S. Chemical and Isotopic Composition of Waters and Dissolved Gases in Some Thermal Springs of Sicily and Adjacent Volcanic Islands, Italy. *Pure Appl. Geophys. PAGEOPH* **2006**, *163*, 781–807. [CrossRef]
11. Stolper, E.; Holloway, J.R. Experimental determination of the solubility of carbon dioxide in molten basalt at low pressure. *Earth Planet. Sci. Lett.* **1988**, *87*, 397–408. [CrossRef]
12. De Gregorio, S.; Camarda, M.; Longo, M.; Cappuzzo, S.; Giudice, G.; Gurrieri, S. Long-term continuous monitoring of the dissolved CO_2. performed by using a new device in groundwater of the Mt. Etna (southern Italy). *Water Res.* **2011**, *45*, 3005–3011. [CrossRef]
13. Irwin, W.P.; Barnes, I. Tectonic relations of carbon dioxide discharges and earthquakes. *J. Geophys. Res. Space Phys.* **1980**, *85*, 3115. [CrossRef]
14. Sugisaki, R.; Ido, M.; Takeda, H.; Isobe, Y.; Hayashi, Y.; Nakamura, N.; Satake, H.; Mizutani, Y. Origin of Hydrogen and Carbon Dioxide in Fault Gases and Its Relation to Fault Activity. *J. Geol.* **1983**, *91*, 239–258. [CrossRef]
15. Klusman, R.W. *Soil Gas and Related Methods for Natural Resource Exploration*; John Wiley and Sons: New York. NY, USA, 1993; p. 483.

16. Italiano, F.; Martinelli, G.; Rizzo, A.L. Geochemical evidence of seismogenic-induced anomalies in the dissolved gases of thermal waters: A case study of Umbria (Central Apennines, Italy) both during and after the 1997-1998 seismic swarm. *Geochem. Geophys. Geosystems* **2004**, *5*. [CrossRef]
17. Ray, M.C.; Hilton, D.; Munoz, J.; Fischer, T.P.; Shaw, A.M. The effects of volatile recycling, degassing and crustal contamination on the helium and carbon geochemistry of hydrothermal fluids from the Southern Volcanic Zone of Chile. *Chem. Geol.* **2009**, *266*, 38–49. [CrossRef]
18. Camarda, M.; De Gregorio, S.; Gurrieri, S. Magma-ascent processes during 2005–2009 at Mt Etna inferred by soil CO_2 emissions in peripheral areas of the volcano. *Chem. Geol.* **2012**, *330*, 218–227. [CrossRef]
19. Camarda, M.; De Gregorio, S.; Di Martino, R.; Favara, R. Temporal and spatial correlations between soil CO_2. flux and crustal stress. *J. Geophys. Res. Solid Earth* **2016**, *121*, 7071–7085. [CrossRef]
20. Chiodini, G.; Frondini, F.; Kerrick, D.; Rogie, J.; Parello, F.; Peruzzi, L.; Zanzari, A. Quantification of deep CO_2. fluxes from Central Italy. Examples of carbon balance for regional aquifers and of soil diffuse degassing. *Chem. Geol.* **1999**, *159*, 205–222. [CrossRef]
21. De Paola, N.; Chiodini, G.; Hirose, T.; Cardellini, C.; Caliro, S.; Shimamoto, T. The geochemical signature caused by earthquake propagation in carbonate-hosted faults. *Earth Planet. Sci. Lett.* **2011**, *310*, 225–232. [CrossRef]
22. Caracausi, A.; Favara, R.; Italiano, F.; Nuccio, P.M.; Paonita, A.; Rizzo, A.L. Active geodynamics of the central Mediterranean Sea: Tensional tectonic evidences in western Sicily from mantle-derived helium. *Geophys. Res. Lett.* **2005**, *32*. [CrossRef]
23. Censi, P.; Ferla, P. I marmi dei Peloritani. Composizione isotopica dell'ossigeno e del carbonio e ricostruzione degli ambienti formazionali. Rend. *Soc. lt. Min. Petr.* **1982**, *38*, 1101–1117.
24. Favara, R.; Grassa, F.; Inguaggiato, S.; D'amore, F. Geochemical and hydrogeological characterization of thermal springs in Western Sicily, Italy. *J. Volcanol. Geotherm. Res.* **1998**, *84*, 125–141. [CrossRef]
25. Favara, R.; Grassa, F.; Inguaggiato, S.; Valenza, M. Hydrogeochemistry and stable isotopes of thermal springs: Earthquake-related chemical changes along Belice Fault (Western Sicily). *Appl. Geochem.* **2001**, *16*, 1–17. [CrossRef]
26. Caracausi, A.; Favara, R.; Italiano, F.; Nuccio, P.M.; Paonita, A.; Rizzo, A. Evidence of mantle derived fluid contributions to the thermal basins of Western Sicily: Geotectonic and geodynamic implications. In *Proceeding of the WRI-11 International Symposium*; Wanty & Seal II, Ed.; Springs: Saratoga, NY, USA, 2004; pp. 91–94.
27. Favara, R.; Grassa, F.; Madonia, P.; Valenza, M. Flow Changes and Geochemical Anomalies in Warm and Cold Springs Associated with the 1992–1994 Seismic Sequence at Pollina, Central Sicily, Italy. *Pure Appl. Geophys. PAGEOPH* **2007**, *164*, 2411–2430. [CrossRef]
28. Dewey, J.F.; Helman, M.L.; Knott, S.D.; Turco, E.; Hutton, D.H.W.; Knott, S.D. Kinematics of the western Mediterranean. Alpine Tectonics. *Geol. Soc. Spec. Publ.* **1989**, *45*, 265–283. [CrossRef]
29. Serpelloni, E.; Vannucci, G.; Pondrelli, S.; Argnani, A.; Casula, G.; Anzidei, M.; Baldi, P.; Gasperini, P. Kinematics of the Western Africa-Eurasia plate boundary from focal mechanisms and GPS data. *Geophys. J. Int.* **2007**, *169*, 1180–1200. [CrossRef]
30. Catalano, S.; De Guidi, G.; Romagnoli, G.; Torrisi, S.; Tortorici, G.; Tortorici, L. The migration of plate boundaries in SE Sicily: Influence on the large-scale kinematic model of the African promontory in southern Italy. *Tectonophys.* **2008**, *449*, 41–62. [CrossRef]
31. Vallone, P.; Giammarinaro, M.; Crosetto, M.; Agudo, M.; Biescas, E. Ground motion phenomena in Caltanissetta (Italy) investigated by InSAR and geological data integration. *Eng. Geol.* **2008**, *98*, 144–155. [CrossRef]
32. 32. Catalano, R.; D'Argenio, B. Schema geologico della Sicilia. In *Guida Alla Geologia Della Sicilia Occidentale*; Catalano, R., D'Argenio, B., Eds.; Guide Geologiche Regionali (I Serie), SOCIETA' GEOLOGICA ITALIANA: Roma, Italy, 1982; pp. 9–41.
33. Roure, F.; Howell, D.; Muller, C.; Moretti, I. Late cenozoic subduction complex of Sicily. *J. Struct. Geol.* **1990**, *12*, 259–266. [CrossRef]
34. Lentini, F.; Carbone, S.; Catalano, S. Main structural domains of the central Mediterranean region and their Neogene tectonic evolution. *Boll. Geofis. Teor. ed Appl.* **1994**, *36*, 141–144.
35. Catalano, R.; Franchino, A.; Merlini, S.; Sulli, A. A crustal section from North Algerian to the Ionian ocean (Central Mediterranean). *Mem. Soc. Geol. It.* **2000**, *55*, 71–85.

36. Finetti, I.R. CROP project: deep seismic exploration of the central Mediterranean and Italy. In *Atlases in Geoscience 1*; Finetti, I.R., Ed.; Elsevier: Amsterdam, The Netherlands, 2005; pp. 1–794.
37. Catalano, R.; Franchino, A.; Merlini, S.; Sulli, A. Central Western Sicily structural setting interpreted from seismic reflection profiles. *Mem. Soc. Geol. It.* **2000**, *55*, 5–16.
38. Ghisetti, F.; Vezzani, L. Thin-skinned deformations of the Western Sicily thrust belt and relationships with crustal shortening: mesostructural data on the Mt. Kumeta Alcantara. *Boll. Soc. Geol. It.* **1984**, *103*, 129–157.
39. Bianchi, F.; Carbone, S.; Grasso, M.; Invernizzi, G.; Lentini, F.; Longaretti, G.; Merlini, S.; Moscardini, F. Sicilia orientale: Profilo geologico Nebrodi-Iblei. *Mem. Soc. Geol. It.* **1989**, *38*, 429–458.
40. Basilone, L. *Litostratigrafia Della Sicilia*; ARTA (Reg. Sicil.)-ORGS. Arti Grafiche Palermitane S.R.L: Palermo, Italy, 2012.
41. Cirrincione, R.; Fiannacca, P.; Lustrino, M.; Romano, V.; Tranchina, A. Late Triassic tholeiitic magmatism in Western Sicily: A possible extension of the Central Atlantic Magmatic Province (CAMP) in the Central Mediterranean area? *Lithos* **2014**, *188*, 60–71. [CrossRef]
42. Patacca, E.; Scandone, P.; Giunta, G.; Liguori, V. Mesozoic palaeotectonic evolution of the Ragusa Zone (Southern Sicily). *Geol. Rom.* **1979**, *18*, 331–369.
43. Longaretti, G.; Rocchi, S. Il magmatismo dell'avampaese ibleo (Sicilia orientale) tra il Trias e il Quaternario: Dati stratigrafici e petrologici del sottosuolo. *Mem Soc Geol Ital.* **1990**, *45*, 911–925.
44. Branca, S.; Coltelli, M.; De Beni, E.; Wijbrans, J. Geological evolution of Mount Etna volcano (Italy) from earliest products until the first central volcanism (between 500 and 100 ka ago) inferred from geochronological and stratigraphic data. *Acta Diabetol.* **2008**, *98*, 239. [CrossRef]
45. Casero, P.; Roure, F. Neogene deformations at the Sicilian–North African plate boundary. In *Peri-Tethian Platforms. Institut Francaise du Petrole Research Conference, Arles, Proceedings*; Roure, F., Ed.; Editions Technip: Paris, France, 1994; pp. 27–50.
46. Cernobori, L.; Hirn, H.; McBride, J.H.; Nicolich, R.; Petronio, M.; Romanelli, M.; Streamers Profiles, Working Group. Crustal image of the Ionian basin and its Calabrian margins. *Tectonophysics* **1996**, *264*, 175–189. [CrossRef]
47. Pondrelli, S.; Piromallo, C.; Serpelloni, E. Convergence vs. retreat in Southern Tyrrhenian Sea: Insights from kinematics. *Geophys. Res. Lett.* **2004**, *31*, 1–4. [CrossRef]
48. Barreca, G.; Bruno, V.; Cocorullo, C.; Cultrera, F.; Ferranti, L.; Guglielmino, F.; Guzzetta, L.; Mattia, M.; Monaco, C.L.; Pepe, F. Geodetic and geological evidence of active tectonic in south-westerm Sicily (Italy). *J. Geodynamic.* **2014**, *82*, 138–149. [CrossRef]
49. Regione Sicilia. Available online: http://www.osservatorioacque.it/?cmd=section&id=9&tpl=default (accessed on 20 May 2020).
50. Liotta, M. Geochemical Processes Governing Groundwater Composition in North-Western Sicily:isotopic Model and Water Rock Interaction. Ph.D. Thesis, University of Palermo, Palermo PA, Italy, 2004; p. 97.
51. Stumm, W.; Morgan, J.J. *Aquatic Chemistry: Chemical Equilibria and Rates in Natural Waters*; Wiley: New York, NY, USA, 1996; p. 1024.
52. Parkhurst, D.L.; Appelo, C.A.J. User's guide to PHREEQC (version 2)—A computer program for speciation, batch-reaction, one-dimensional transport, and inverse geochemical modelling calculations. In *U.S. Geological Survey Water—Resources Investigations Report*; United States Geological Survey: Reston, VA, USA, 1999; pp. 99–4259. 312p.
53. Rovida, A.; Locati, M.; Camassi, R.; Lolli, B.; Gasperini, P. (Eds.) *CPTI15, the 2015 Version of the Parametric Catalogue of Italian*; Earthquakes. Istituto Nazionale di Geofisica e Vulcanologia: Rome, Italy, 2016. [CrossRef]
54. Madonia, P.; Liotta, M. Chemical composition of precipitation at Mt. Vesuvius and Vulcano Island, Italy: Volcanological and environmental implications. *Environ. Earth Sci.* **2009**, *61*, 159–171. [CrossRef]
55. Liotta, M.; D'Alessandro, W.; Bellomo, S.; Brusca, L. Volcanic plume fingerprint in the groundwater of a persistently degassing basaltic volcano: Mt. Etna. *Chem. Geol.* **2016**, *433*, 68–80. [CrossRef]
56. Dongarraa, G.; Manno, E.; Sabatino, G.; Varrica, D. Geochemical char- acteristics of waters in mineralised area of Peloritani Mountains (Sicily, Italy). *Appl. Geochem.* **2009**, *24*, 900–914. [CrossRef]
57. Di Stefano, P.; Favara, R.; Luzio, D.; Renda, P.; Cacciatore, M.S.; Calo', M.; Napoli, G.; Parisi, L.; Todaro, S.; Zarcone, G. A regional-scale discontinuity in western Sicily revealed by a multidisciplinary approach: A new piece for understanding the geodynamic puzzle of the southern Mediterranean. *Tectonics* **2015**, *34*, 2067–2085. [CrossRef]

58. Palano, M.; Schiavone, D.; Loddo, M.; Neri, M.; Presti, D.; Quarto, R.; Totaro, C.; Neri, G. Active upper crust deformation pattern along the southern edge of the Tyrrhenian subduction zone (NE Sicily): Insights from a multidisciplinary approach. *Tectonophysics* **2015**, *657*, 205–218. [CrossRef]
59. Bonforte, A.; Catalano, S.; Maniscalco, R.; Pavano, F.; Romagnoli, G.; Sturiale, G.; Tortorici, G. Geological and geodetic constraints on the active deformation along the northern margin of the Hyblean Plateau (SE Sicily). *Tectonophysics* **2015**, *640*, 80–89. [CrossRef]
60. Caracausi, A.; Italiano, F.; Paonita, A.; Rizzo, A.; Nuccio, P.M. Evidence of deep magma degassing and ascent by geochemistry of peripheral gas emissions at Mount Etna (Italy): Assessment of the magmatic reservoir pressure. *J. Geophys. Res. Space Phys.* **2003**, *108*, 2463. [CrossRef]
61. Rizzo, A.L.; Caracausi, A.; Favara, R.; Martelli, M.; Paonita, A.; Paternoster, M.; Nuccio, P.M.; Rosciglione, A. New insights into magma dynamics during last two eruptions of Mount Etna as inferred by geochemical monitoring from 2002 to 2005. *Geochem. Geophys. Geosystems* **2006**, *7*. [CrossRef]
62. DISS Working Group. Database of Individual Seismogenic Sources (DISS), Version 3.2.1: A Compilation of Potential Sources for Earthquakes Larger than M 5.5 in Italy and Surrounding Areas. 2018. Available online: http://diss.rm.ingv.it/diss/ (accessed on 16 April 2019). [CrossRef]
63. Lentini, F.; Carbone, S. Geologia della Sicilia. In *Memorie Descrittive della Carta Geologica d'Italia*; XCV. ISPRA—Servizio Geologico d'Italia: Roma, Italy, 2014.
64. Liotta, M.; Martelli, M. Dissolved gases in brackish thermal waters: An improved analytical method. *Geofluids* **2012**, *12*, 236–244. [CrossRef]
65. Liotta, M.; D'Alessandro, W.; Arienzo, I.; Longo, M. Tracing the circulation of groundwater in volcanic systems using the 87Sr/86Sr ratio: Application to Mt. Etna. *J. Volcanol. Geotherm. Res.* **2017**, *331*, 102–107. [CrossRef]